

# Screening of resonant magnetic perturbation penetration by flows in tokamak plasmas based on two-fluid model

Weikang Tang (汤炜康), Zheng-Xiong Wang (王正汹), Lai Wei (魏来), Shuangshuang Lu (路爽爽), Shuai Jiang (姜帅) and Jian Xu (徐健)

Key Laboratory of Materials Modification by Laser, Ion, and Electron Beams (Ministry of Education), School of Physics, Dalian University of Technology, Dalian 116024, People's Republic of China

E-mail: zxwang@dlut.edu.cn

**Abstract.** Numerical simulation on the resonant magnetic perturbation penetration is carried out by the newly-updated initial value code MDC (MHD@Dalian Code). Based on a set of two-fluid four-field equations, the bootstrap current, parallel and perpendicular transport effects are included appropriately. Taking into account the bootstrap current, a mode penetration like phenomenon is found, which is essentially different from the classical tearing mode model. It may provide a possible explanation for the finite mode penetration threshold at zero rotation detected in experiments. To reveal the influence of diamagnetic drift flow on the mode penetration process,  $\mathbf{E} \times \mathbf{B}$  drift flow and diamagnetic drift flow are separately applied to compare their effects. Numerical results show that, a sufficiently large diamagnetic drift flow can drive a strong stabilizing effect on the neoclassical tearing mode. Furthermore, an oscillation phenomenon of island width is discovered. By analyzing in depth, it is found that, this oscillation phenomenon is due to the negative feedback regulation of pressure on the magnetic island. This physical mechanism is verified again by key parameter scanning.

*Keywords:* tokamak, two-fluid plasma, NTM

## 1. Introduction

Tearing mode (TM) instability is extensively investigated by researchers in the area of tokamak plasmas in the recent decades [1, 2]. The TM is one kind of current driven magnetohydrodynamic (MHD) instabilities commonly followed by the magnetic reconnection, which can break up the nested magnetic flux surfaces and generate magnetic islands at corresponding resonant surface. These magnetic islands can provide a “seed”, called seed island, for the neoclassical tearing mode (NTM) to grow. NTM, a pressure gradient driven MHD instability, is linearly stable but can be destabilized by helical perturbations due to the loss of bootstrap current inside the seed island [3]. The onset of NTM is the principal limitation of the plasma temperature in the core region [4], owing to the radial “shortcut” transport in the produced large magnetic island, and one of the main cause of major disruption [5, 6]. For the sake of economic feasibility, a high fraction of bootstrap current, up to 80-90%, is required for future advanced tokamak. Since NTM is a high beta phenomenon, which is proportional to the bootstrap current fraction, the control and suppression of NTM is of great significance for the steady state operation of tokamak devices [7–9].

Aiming to control the NTM, many research efforts have been dedicated to the resonant magnetic perturbation (RMP) since the 1990s [10–14]. RMP has been found to drive additional effects on magnetic islands in tokamak plasmas. Specifically, the RMP can produce an electromagnetic torque at the corresponding resonant surface. Once the electromagnetic torque is sufficiently large to balance the plasma viscosity and inertia torque, the magnetic islands would be compulsorily aligned with the RMP in a identical frequency, called locked mode (LM) [15]. For a static RMP, it can be used to test the maximum tolerance for the residual error field, resulting from the asymmetry of the tokamak device [16, 17]. As for the dynamic RMP, it can be utilized to unlock the magnetic island and maintain a stable toroidal and poloidal rotation [18]. Lately, experimental and numerical results show that the synergetic application of RMP and electron cyclotron current drive (ECCD) is a promising and effective method to control the NTM [19–21]. The RMP can be used as an auxiliary method to lock and locate the phase of the NTM, and then to enhance the accuracy and effectiveness of the ECCD.

In addition to above application, even if the rotating plasma is originally stable to the NTM, the RMP can drive magnetic reconnection and generate magnetic island at the resonant surface, called mode penetration [22, 23]. Mode penetration has raised much concern, since its threshold is directly related to the onset of TM/NTM. Based on single-fluid theory, considerable studies have been made in predicting and explaining the threshold of mode penetration for different tokamak devices and parameter regimes [24–27]. However, considering the plasma rotation playing a significant role in the screening process of RMP [28], the two-fluid model, retaining the electron diamagnetic drift as well as the  $\mathbf{E} \times \mathbf{B}$  flow, is more suitable to account for more complex physics. Recently, in the frame of the two-fluid drift-MHD theory, plenty of researches were carried out to investigate the interaction of the RMP and magnetic islands in tokamak

plasmas [29–32]. Using a two-fluid model, Hu *et al* found that the two-fluid effects can give significant modifications to the scaling law of mode penetration for different plasma parameters. Besides, the enduring mystery that non-zero penetration threshold at zero plasma natural frequency is explained by the small magnetic island width when penetrated [33,34]. On the other hand, in this paper, taking into account the bootstrap current, a mode penetration like process is found by numerical simulation. It may provide another possible explanation for the enduring mystery. Furthermore, the effect of diamagnetic drift flow on the mode penetration is studied numerically. It is found that the diamagnetic drift flow has a stabilizing effect on the magnetic islands. An oscillation phenomenon of island width is discovered in high Lundquist number  $S$  and high transport scenario.

The rest of this paper is organized as follows. In section 2, the modeling equations used in this work are introduced. In section 3, numerical results and physical discussions are presented. Finally, the paper is summarized and conclusions are drawn in section 4.

## 2. Physical model

The initial value code MDC (MHD@Dalian Code) [35–39] is upgraded to the two fluid version based on a set of four-field MHD equations [40]. Taking into account the nonlinear evolution of the vorticity  $U$ , the poloidal magnetic flux  $\psi$ , the plasma pressure  $p$  and the parallel ion velocity  $v$ , the normalized equations in the cylindrical geometry  $(r, \theta, z)$  can be written as

$$\frac{\partial U}{\partial t} = [U, \phi + \delta \tau p] + \nabla_{\parallel} j + \nu \nabla_{\perp}^2 U + \delta \tau [\nabla_{\perp} p, \nabla_{\perp} u], \quad (1)$$

$$\frac{\partial \psi}{\partial t} = -\nabla_{\parallel} \phi + \delta \nabla_{\parallel} p - \eta(j - j_b), \quad (2)$$

$$\frac{\partial p}{\partial t} = [p, \phi] + 2\beta_e \delta \nabla_{\parallel} j - \beta_e \nabla_{\parallel} v + \chi_{\parallel} \nabla_{\parallel}^2 p + \chi_{\perp} \nabla_{\perp}^2 p, \quad (3)$$

$$\frac{\partial v}{\partial t} = [v, \phi] - \frac{1}{2}(1 + \tau) \nabla_{\parallel} p + \mu \nabla_{\perp}^2 v, \quad (4)$$

where  $\phi$  and  $j$  are, respectively, the electric potential and plasma current density along the axial direction, obtaining by the following formulas  $U = \nabla_{\perp}^2 \phi$  and  $j = -\nabla_{\perp}^2 \psi$ . The equation (1) (vorticity equation) is the perpendicular component (taking  $e_z \cdot \nabla \times$ ) of the equation of motion, where  $\nu$  is the viscosity and  $\tau = T_i/T_e$  is the ratio of ion to electron temperature.  $\delta = (2\Omega_i \tau_a)^{-1}$  is a gyroradius parameter, also known as ion skin depth, where  $\Omega_i = eB_0/m_i$  is a constant measure of the ion gyrofrequency and  $\tau_a = \sqrt{\mu_0 \rho} a/B_0$  is Alfvén time. Neglecting the electron inertia and Hall effect, the equation (2) is obtained by combining the generalized Ohm’s law and Faraday’s law of electromagnetic induction, where  $\eta$  is the resistivity.  $j_b = -A\sqrt{\varepsilon}/B_{\theta} p'(r)$  is the bootstrap current [41], where  $\varepsilon = a/R_0$  is the inverse aspect-ratio, and  $B_{\theta}$  is the poloidal magnetic field.  $A$  is a constant that can be calculated by a given bootstrap current fraction

$f_b = \int_0^a j_b r dr / \int_0^a j r dr$ . Since isothermal assumption is made here, the evolution of pressure is mainly determined by the particle conservation law. It is basically a transport equation, considering the convective term, parallel and perpendicular heat transport. By including the effect of resistive diffusion and the parallel ion flow, the equation (3) is the final energy transport equation for two-fluid plasma.  $\beta_e = 2\mu_0 n_0 T_e / B_0^2$  is the electron plasma beta at the location of magnetic axis, where  $T_e$  is the constant electron temperature.  $\chi_{\parallel}$  and  $\chi_{\perp}$  are the parallel and perpendicular transport coefficients, respectively. The equation (4) is the parallel component of the equation of motion by taking the dot product of the equation with  $\mathbf{B}$ , where  $\mu$  is the diffusion coefficient of parallel ion velocity.

The radial coordinate  $r$ , time  $t$ , and velocity  $v$  are normalized by the plasma minor radius  $a$ , Alfvén time  $\tau_a$  and Alfvén speed  $v_a = B_0 / \sqrt{\mu_0 \rho}$ , respectively. The poloidal magnetic flux  $\psi$ , electric potential  $\phi$  and plasma pressure  $p$  are normalized by  $aB_0$ ,  $aB_0 v_a$  and the pressure at the magnetic axis  $p_0$ , respectively. The Poisson brackets in equations (1)-(4) are defined as

$$[f, g] = \nabla f \times \nabla g \cdot \hat{z} = \frac{1}{r} \left( \frac{\partial f}{\partial r} \frac{\partial g}{\partial \theta} - \frac{\partial g}{\partial r} \frac{\partial f}{\partial \theta} \right). \quad (5)$$

Each variable  $f(r, \theta, z, t)$  in equations (1)-(4) can be written in the form  $f = f_0(r) + \tilde{f}(r, \theta, z, t)$  with  $f_0$  and  $\tilde{f}$  being the time-independent initial profile and the time-dependent perturbation, respectively. By applying the periodic boundary conditions in the poloidal and axial directions, the perturbed fields can be Fourier-transformed as

$$\tilde{f}(r, \theta, z, t) = \frac{1}{2} \sum_{m,n} \tilde{f}_{m,n}(r, t) e^{im\theta - inz/R_0}, \quad (6)$$

with  $R_0$  being the major radius of the tokamak.

The effect of RMP with  $m/n$  is taken into account by the boundary condition

$$\tilde{\psi}_{m,n}(r=1) = \psi_a(t) e^{im\theta - inz/R_0}. \quad (7)$$

In this way, the perturbed radial magnetic field at plasma boundary over toroidal magnetic field could be calculated by  $\delta B_r / B_0 = am\psi_a$ . It should be pointed out that, in a real tokamak, the toroidal rotation is prevailing and much stronger than the poloidal one, whereas only the poloidal rotation is considered in this work. Considering the fact that the electromagnetic force exerted in the poloidal direction is  $(n/m)(r_s/R)$  times smaller than that in toroidal direction, and the speed in toroidal direction should be  $(m/n)(R/r_s)$  times larger than the poloidal one for having an equivalent rotation frequency, the locking threshold in the toroidal direction can, therefore, be estimated by multiplying such a factor  $[(m/n)(R/r_s)]^2$ .

Given the initial profiles of  $\phi_0$ ,  $\psi_0$ ,  $p_0$  and  $v_0$ , equations (1)-(4) can be solved simultaneously by our code MDC. The two-step predictor-corrector method is applied in the time advancement. The finite difference method is used in the radial direction and the pseudo-spectral method is employed for the poloidal and the toroidal directions ( $\theta, \zeta = -z/R_0$ ).

### 3. Simulation results

#### 3.1. Numerical set-up

Consider a low density ohmically heated tokamak discharge with electron density  $n_e \approx 2 \times 10^{19} \text{ m}^{-3}$ , toroidal magnetic field  $B_0 = 2 \text{ T}$  and inverse aspect ratio  $\varepsilon = a/R_0 = 0.5\text{m}/2\text{m} = 0.25$ . This will lead to the Alfvén speed  $v_a \approx 6.9 \times 10^6 \text{ m/s}$  and Alfvén time  $\tau_a \approx 7.24 \times 10^{-8} \text{ s}$ . The corresponding Alfvén frequency is  $\omega_a \approx 1.38 \times 10^7 \text{ Hz}$ . Otherwise stated, other plasma parameters are set as follow,  $\tau = 1$ ,  $\beta_e = 0.01$ ,  $\eta = 10^{-6}$ ,  $\nu = 10^{-7}$ ,  $\mu = 10^{-6}$ ,  $\chi_{\parallel} = 10$  and  $\chi_{\perp} = 10^{-6}$ . The radial mesh number is set as  $N_r = 2048$ . In this work, the nonlinear simulations only include single helicity perturbations with higher harmonics ( $m/n=3/2$ ,  $0 \leq m \leq 18$ ), in addition to the changes in the equilibrium quantities ( $m/n=0/0$  component). To simulate the mode penetration process, a linearly stable equilibrium safety factor  $q$  profile and the normalized plasma pressure  $p$  profile are given in figure 1, with the  $q = 3/2$  resonant surface located at  $r = 0.402$ .

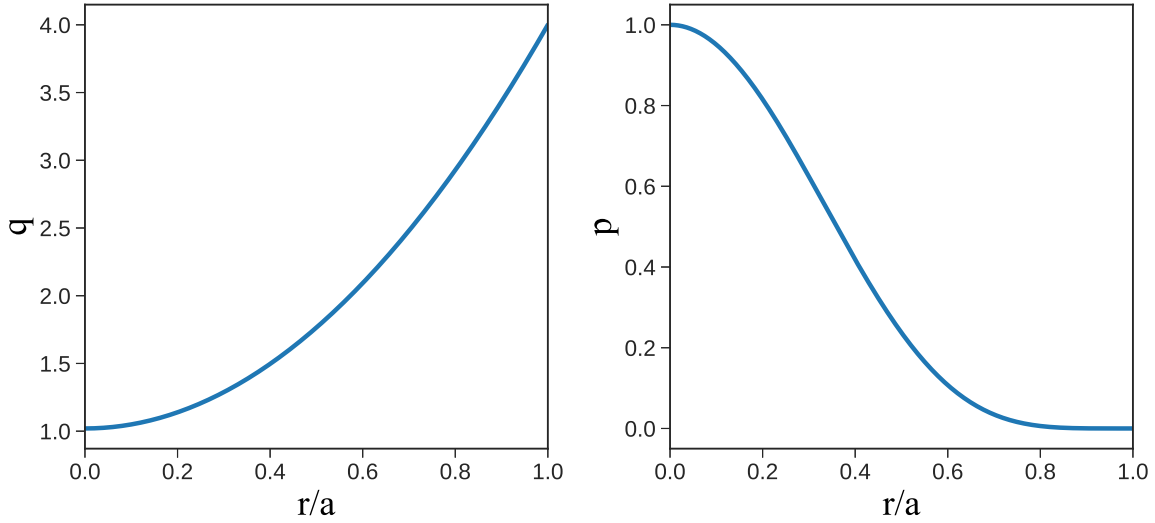


**Figure 1.** Safety factor  $q$  and pressure  $p$  profiles adopted in this work.

#### 3.2. Basic verification

To begin with, the role of seed island width on the onset of NTM is verified to ensure the neoclassical current effect implemented properly. The seed island width is considered by the initial magnetic perturbation in a form of  $\tilde{\psi}_{t=0} = \psi_{00}(1-r)^2$ . The nonlinear evolution of magnetic island width for different initial magnetic perturbations are presented in the left panel of figure 2. The solid traces are for bootstrap current fraction  $f_b = 0.3$  (NTM) and dotted one for  $f_b = 0.0$  (TM). For the classical TM, even a very large seed island width is given, the island width still fades with time, illustrating that the TM in this  $q$  profile is linearly stable. Taking the bootstrap current into consideration, it is seen that there is a threshold for the mode to grow, manifesting that the nonlinearly unstable NTM

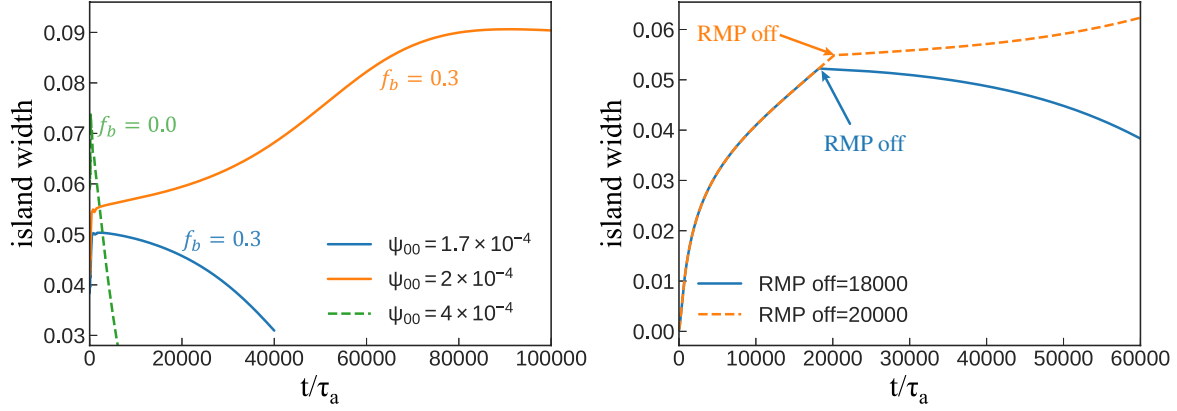


**Figure 2.** (left) Nonlinear evolution of the island width for different magnitude of seed island. The solid traces are for bootstrap current fraction  $f_b = 0.3$  and the dashed trace is for  $f_b = 0$ . (right) Nonlinear evolution of island width for different turn-off time of RMP with  $f_b = 0.3$  and  $\delta B_r/B_0 = 3.75 \times 10^{-5}$ .

is triggered for a larger seed island width. In experiments, the RMP coils are commonly used to seed a magnetic island. Then the onset of NTM by RMP is tested. The RMP is turned on from the very beginning with the amplitude of  $\delta B_r/B_0 = 3.75 \times 10^{-5}$ . In figure 2 (right), in the presence of RMP, the nonlinear evolution of island width for  $f_b = 0.3$  is shown. After applying the RMP, the originally stable TM can be forced driven unstable, as the island width grows even without any seed island. Then the RMP is turned off at different time when island width grows to a moderate magnitude, to testify if it is the driven reconnection or the onset of NTM. It turns out that, if the RMP is turned off before the island width is sufficiently large, the magnetic island still could not grow spontaneously. It confirms again that the existence of the critical island width for triggering the NTM, which is consistent with the theory.

### 3.3. Comment on the “enduring mystery”

Based on the above results, effects of different RMP amplitudes are then scanned for  $f_b = 0.0$  and  $f_b = 0.3$  with zero rotation (electric drift  $\omega_E$  and diamagnetic drift  $\omega_{\text{dia}}$  are both zero). For  $f_b = 0.0$  (figure 3 left), the saturated island width is positively related to the RMP amplitude, a typical driven reconnection. However, for  $f_b = 0.3$  (figure 3 right), a mode penetration like phenomenon can be observed. If the RMP amplitude is relatively small, the magnetic island is going to saturate at a very small magnitude. Once the RMP amplitude is sufficiently large, the final island width would be very large and keep almost the same even further increasing the RMP amplitude. This phenomenon is consistent with the “enduring mystery in experiments” reported by Hu *et al*, i.e. non-zero penetration threshold at zero plasma natural frequency [33, 34]. On the other hand, this phenomenon is different from the so-called mode penetration, and we will demonstrate it next.

Corresponding to figure 3 (right), the saturated magnetic island width is shown

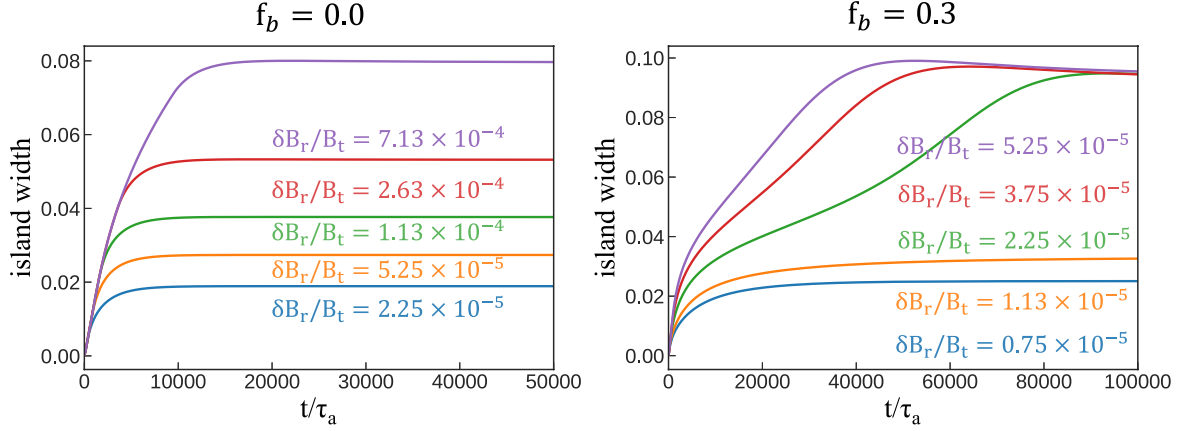


**Figure 3.** Temporal evolution of island width for different RMP amplitude for bootstrap current fraction  $f_b = 0$  (left) and  $f_b = 0.3$  (right) without plasma rotation.

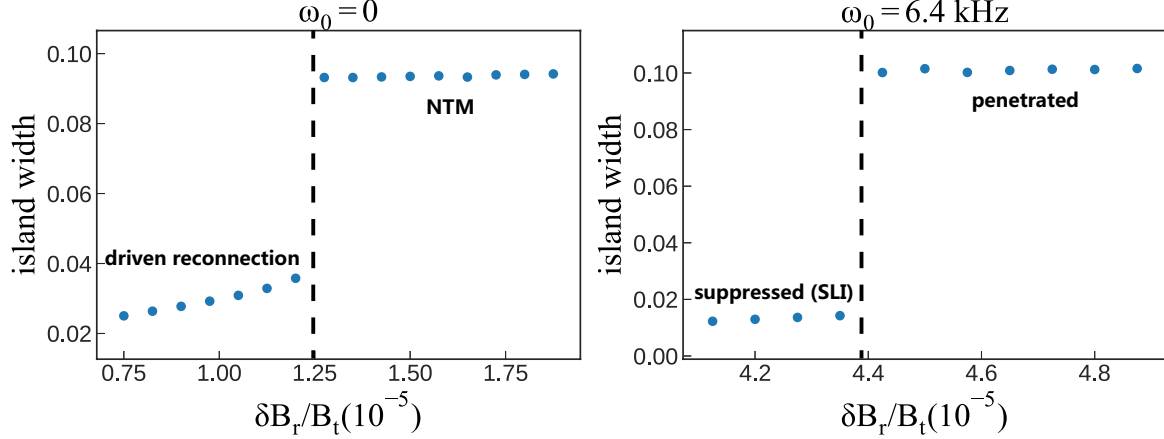


**Figure 4.** Island width versus the RMP amplitude for natural frequency  $\omega_0 = 0$  (left) and  $\omega_0 = 6.4$  kHz (right). The bootstrap current fraction  $f_b$  is set as 0.3.

as a function of RMP amplitude in figure 4 (left). As the RMP amplitude increases, the saturated island width increases slowly first. Once the RMP amplitude exceeds a threshold, there is a jump of the saturated island width. This process can be divided into two parts, i.e. the driven reconnection phase for smaller RMPs and the onset of NTM for large RMPs. Next, including the effect of equilibrium  $\mathbf{E} \times \mathbf{B}$  flow, scan over the RMP amplitude is performed again. The equilibrium  $\mathbf{E} \times \mathbf{B}$  flow is considered by a poloidal momentum source  $\Omega_s(r) = 1/r * d\phi_0/dr$ . Here,  $\delta$  is set to be zero, so only the  $\mathbf{E} \times \mathbf{B}$  flow is considered. For a 6.4 kHz plasma rotation, the saturated island width versus the RMP amplitude is presented in figure 4 (right). This is a typical mode penetration case, as the RMP amplitude increases above a threshold, the island width boosts to a large magnitude. There is one main distinction between the left and right panel of figure 4, even though they look similar. That is, below the threshold, the island width barely changes for the case with plasma rotation but slowly increases for

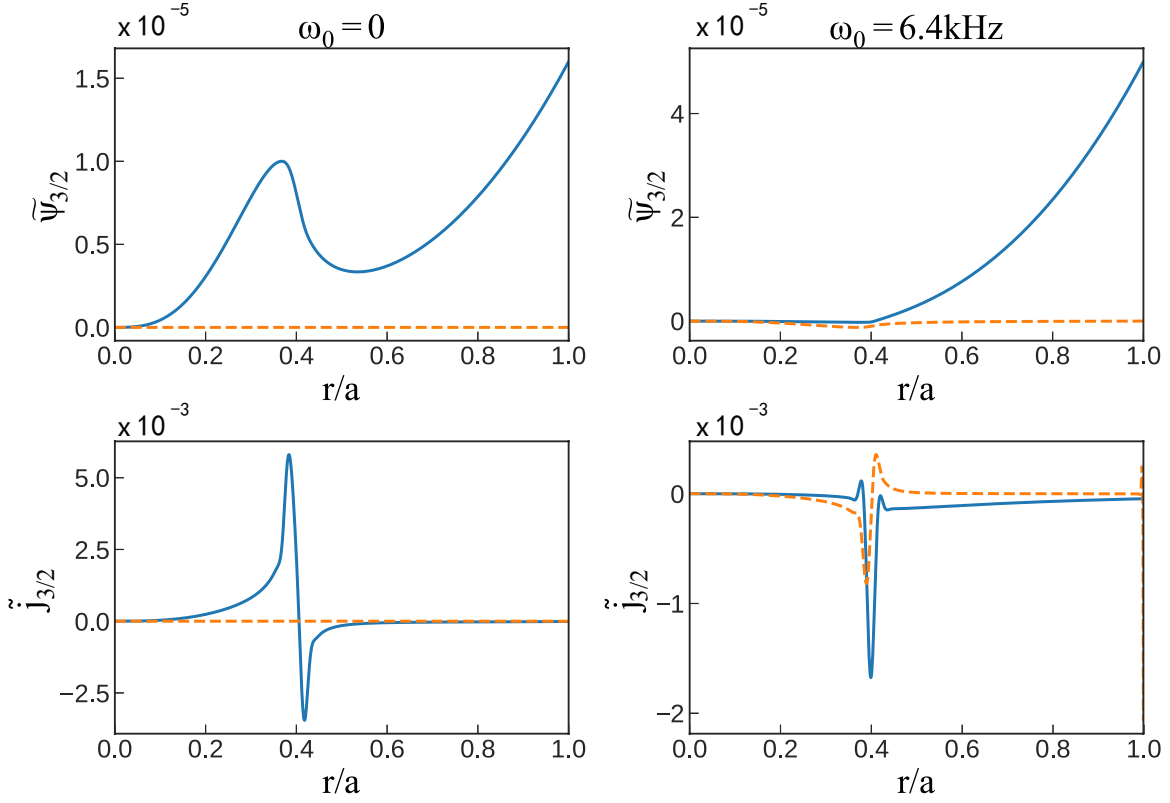


**Figure 5.** The typical eigenmode structure of poloidal magnetic flux and current density for  $m/n=3/2$  component in the regime below the jump of island width. For natural frequency  $\omega_0 = 0$  (left column), the magnetic perturbation in the core region is excited by the RMP. For  $\omega_0 = 6.4$  kHz (right column), the RMP is kept out from the resonant surface. The solid traces are for the real part and dashed traces for the imaginary part.

the case without rotation. The increase regime for the case without rotation is due to the forced reconnection driven by the externally applied RMP. However, the regime below the threshold for the case with rotation is because of the screening effect of the plasma flow. The corresponding eigenmode structures of perturbed poloidal magnetic flux and current density for the case without/with plasma rotation are plotted in the left/right column of figure 5, respectively. It can be clearly observed that the RMP is screened inside the resonant surface for the case with rotation, from the fact that the magnetic perturbation is nearly zero for  $r < r_s$ . In addition, a strong shielding current is formed at the resonant surface, which is consistent with the experimental results on TEXTOR tokamak [42]. These characteristics are the same as the small locked island (SLI) observed in J-TEXT tokamak [43, 44], indicating that the SLI is a suppressed state before the mode penetration. In Fitzpatrick's linear theory [22], the transition from the linear suppressed island to the non-linear island state is irreversible, i.e. in the linear response there is only downward bifurcation [45]. However, the SLI is a phenomenon that a non-linear magnetic island return to the linear state where the

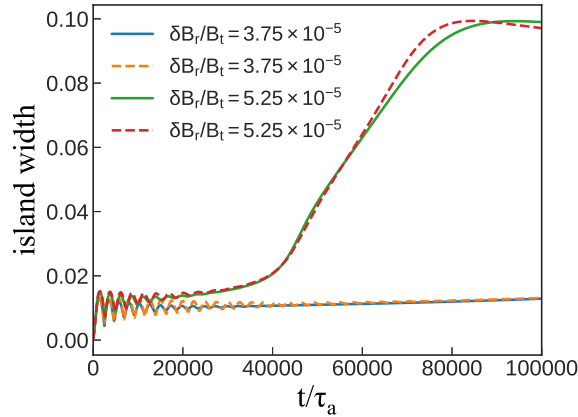


island is suppressed. Thus, perhaps the branch of this kind of upward bifurcation is missed in the previous theory. For the case without rotation, other other hand, the  $m/n = 3/2$  component of magnetic perturbation is induced and kept by the  $3/2$  RMP at the boundary.

All in all, the above simulation results may provide another possible explanation for the “enduring mystery”; considering the effect of bootstrap current, the onset of NTM can lead to a mode penetration like phenomenon, a driven connection regime plus a NTM regime. As a result, it seems there is a finite threshold for mode penetration if not carefully distinguished.

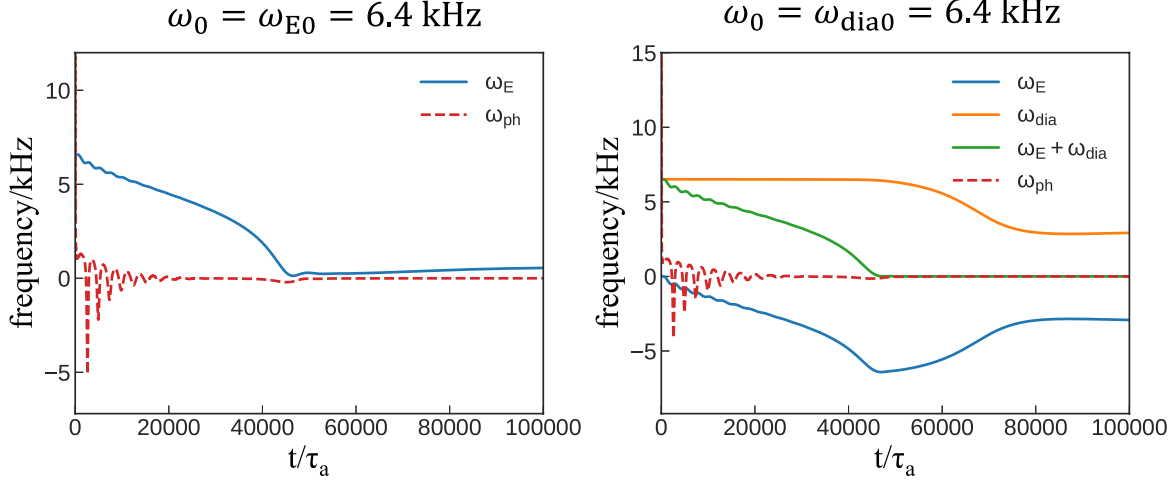
### 3.4. Effects of diamagnetic drift flow

In this subsection, effects of diamagnetic drift flow on the RMP penetration are numerically studied in comparison with the  $\mathbf{E} \times \mathbf{B}$  electric drift flow. The equilibrium  $\mathbf{E} \times \mathbf{B}$  flow velocity can be directly obtained by  $v_{E0} = \partial\phi_0/\partial r$ , and the equilibrium electron diamagnetic flow velocity can be calculated by  $v_{dia0} = -\delta\partial p_0/\partial r$ , where the subscript 0 is for equilibrium quantities. Therefore, the natural plasma rotation could be obtained by the sum of these two effects. By changing the value of  $\delta$ , different amplitude of diamagnetic drift flow can be implemented.

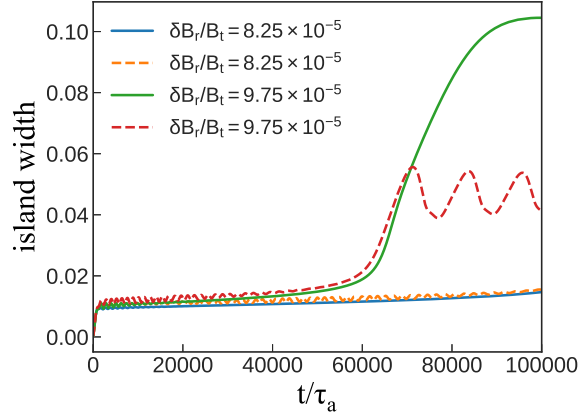


**Figure 6.** Nonlinear evolution of the island width for  $\omega_0 = \omega_{E0} = 6.4$  kHz (solid) and  $\omega_0 = \omega_{dia0} = 6.4$  kHz (dashed).

As shown in figure 6, the screening effects of the two types of flow on the RMP penetration are compared. The solid lines are for cases with a equilibrium  $\mathbf{E} \times \mathbf{B}$  flow frequency  $\omega_{E0} = 6.4$  kHz and diamagnetic flow frequency  $\omega_{dia0} = 0$ , while dotted lines for  $\omega_{dia0} = 6.4$  kHz and  $\omega_{E0} = 0$ . Thus, for both cases the natural frequency is  $\omega_0 = \omega_{E0} + \omega_{dia0} = 6.4$  kHz. It makes no difference on the penetration threshold, no matter what kind of the flow it is, which means the penetration threshold only depends on the rotation difference between the resonant surface and the RMP. Corresponding to the two penetrated case in figure 6, the temporal evolution of the flow frequencies  $\omega_E$ ,  $\omega_{dia}$ ,  $\omega_E + \omega_{dia}$  and the frequency of the phase of the island  $\omega_{ph}$  is illustrated in



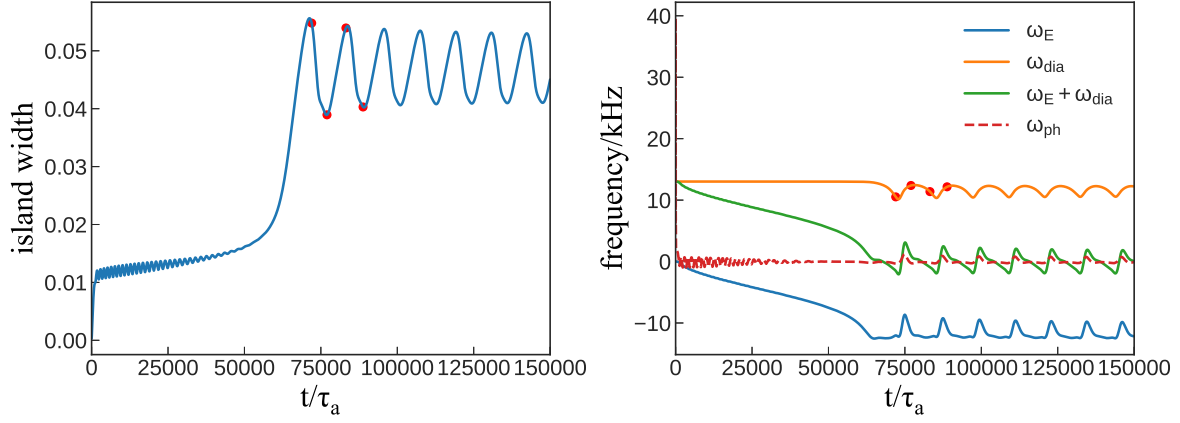
**Figure 7.** Temporal evolution of the phase frequency  $\omega_{ph}$  and different flow frequency  $\omega_E$ ,  $\omega_{dia}$  and  $\omega_{tot} = \omega_E + \omega_{dia}$ . The  $\omega_{ph}$  is calculated by the partial derivative of the phase of poloidal flux  $\Phi_\psi$  with respect to time.  $\omega_E$  and  $\omega_{dia}$  are the angular frequencies of electric drift and diamagnetic drift flow, respectively.



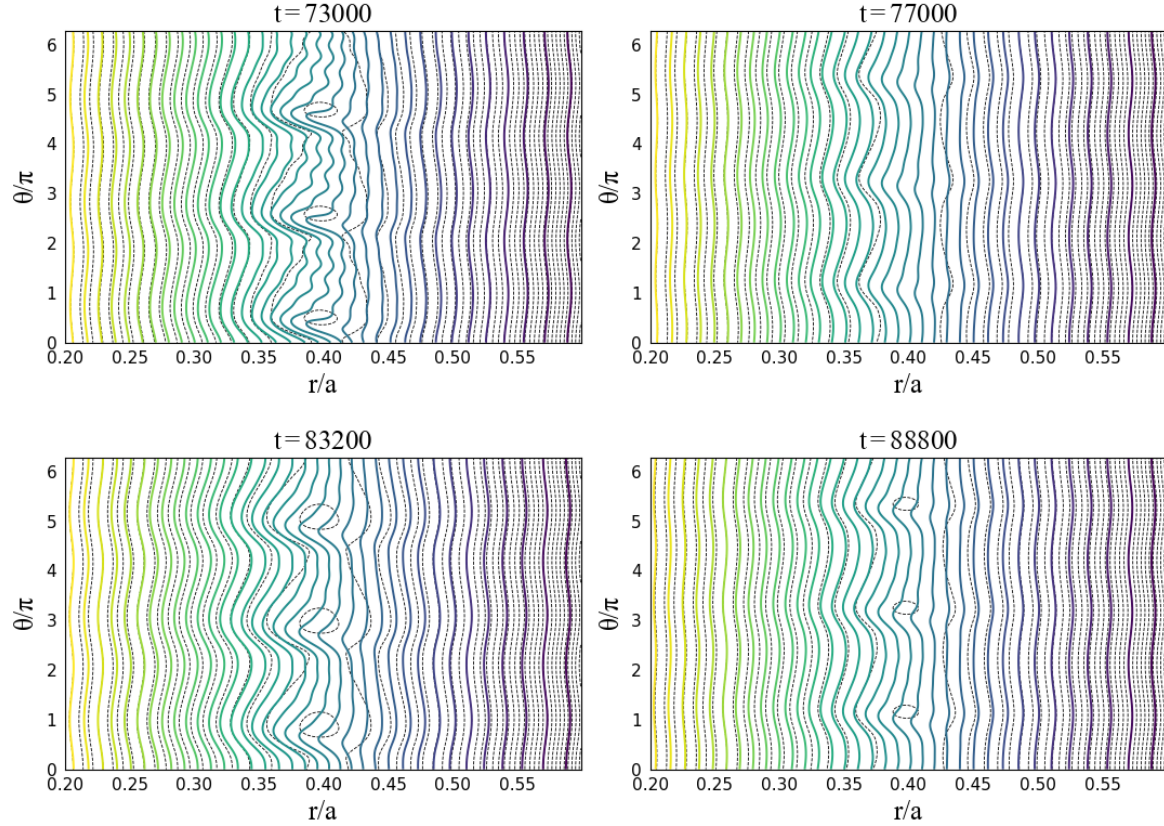
**Figure 8.** Nonlinear evolution of the island width for  $\omega_0 = \omega_{E0} = 12.8$  kHz (solid) and  $\omega_0 = \omega_{dia0} = 12.8$  kHz (dashed).

figure 7. It shows a good agreement for the flow frequency and the phase frequency after mode penetration, indicating that the magnetic island and the flow are coupled in accordance with the frozen-in theorem. For the case ( $\omega_{E0} = 6.4$  kHz,  $\omega_{dia0} = 0$ ), the  $\omega_E$  decreases with time and drops to zero at the moment penetration occurs. For the case ( $\omega_{E0} = 0$ ,  $\omega_{dia0} = 6.4$  kHz), since the  $\omega_{dia}$  is a rigid flow effect which is mainly proportional to the pressure gradient, it doesn't change at the beginning but starts to decrease as the magnetic island grows, where the pressure gradient is flattened. In consequence, the  $\omega_E$  will rotate at the opposite direction to cancel the diamagnetic flow.

When it comes to a larger rotation frequency, the situation is somewhat different. Similar to figure 6, the nonlinear evolution of the island width for a larger natural frequency  $\omega_0 = 12.8$  kHz is presented in figure 8. It shows again that the penetration



**Figure 9.** Temporal evolution of the island width and various frequencies for the oscillated case ( $\omega_0 = \omega_{\text{dia}0} = 12.8$  kHz,  $\delta B_r/B_0 = 9.75 \times 10^{-5}$ ) in figure 8. Oscillation of  $\omega_{\text{dia}}$  is observed after mode penetration. Four time points  $t=73000$ ,  $t=77000$ ,  $t=83200$  and  $t=88800$  are marked by the red circles.



**Figure 10.** Contour plot of the plasma pressure  $p$  (solid lines) and poloidal flux  $\psi$  (dotted lines), corresponding to the four red time points marked in figure 9.

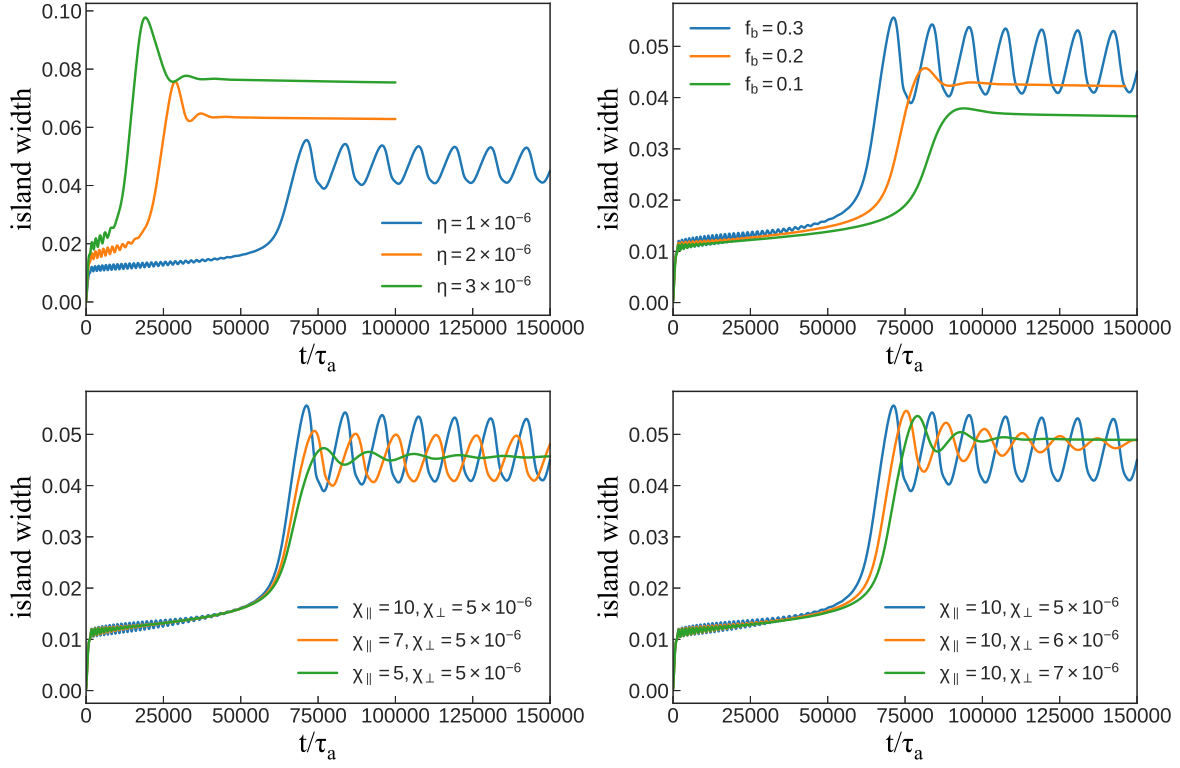


**Figure 11.** Comparison of island width versus time for different (upper left) resistivity  $\eta$ , (upper right) bootstrap current fraction  $f_b$ , (lower left) parallel transport coefficient  $\chi_{\parallel}$  and (lower right) perpendicular transport coefficient  $\chi_{\perp}$ .

threshold is almost the same. However, there are two differences observed. First, the saturated island width is evidently smaller for the case ( $\omega_{E0}=0$ ,  $\omega_{dia0}=12.8$  kHz) than that of the case ( $\omega_{E0}=12.8$  kHz,  $\omega_{dia0}=0$ ), implying that the diamagnetic flow can drive a stabilizing effect on the magnetic island. Second, an oscillation phenomenon of the magnetic island is discovered after mode penetration. To further analyze this oscillation phenomenon, the island width and flow frequency of the oscillated case in figure 8 are plotted, as shown in figure 9. The periodical oscillation of diamagnetic flow frequency is observed as well in figure 9 (right). It should be noted that the oscillation of frequency lags behind the island width a bit, suggesting that the change of island width results in the change of the diamagnetic flow frequency at first. Since the diamagnetic flow is proportional to the pressure gradient, it can be straightforwardly inferred that this phenomenon is related to the change of plasma pressure. To proceed a further step, the contour plot of the pressure  $p$  together with the poloidal magnetic flux  $\psi$  is shown in figure 10, corresponding to the four red time points in figure 9. As the magnetic island grows larger ( $t=73000$  and  $t=83200$ ), the pressure gradient  $\nabla_{\parallel}p$  with respect to the magnetic field inside the island becomes larger. For a smaller island width ( $t=77000$  and  $t=88800$ ), on the contrary, the  $\nabla_{\parallel}p$  is smaller. This modification of pressure gradient can in return affect the island width by the  $\delta \nabla_{\parallel}p$  term in equation (2), leading to the

above oscillation phenomenon.

In order to further verify our conjecture, the effect of resistivity  $\eta$  is then investigated. For a larger  $\eta$ , it turns out that the oscillation phenomenon disappears and the island width recovers as illustrated in figure 11 (upper left). It can be easily understood through equation (2). Since  $\eta$  is a diffusive term, the effect of  $\delta\nabla_{\parallel}p$  term, stabilizing the island and causing the oscillation, can be diffused to some extent with the increasing  $\eta$ , in much the same way as viscosity  $\nu$  in the vorticity equation stabilizing the oscillation of rotation. In other words, the oscillation phenomenon is a result of the competition of the two terms  $\delta\nabla_{\parallel}p$  and  $\eta(j - j_b)$ . For the same reason, a smaller bootstrap current fraction  $f_b$  can remove the oscillation by making the  $\eta(j - j_b)$  term larger, shown in figure 11 (upper right). As the ratio of parallel to perpendicular transport coefficient  $\chi_{\parallel}/\chi_{\perp}$  is crucial to the process of pressure evolution, the effect of different  $\chi_{\parallel}$  and  $\chi_{\perp}$  values are studied. In figure 11 (lower left and right), the temporal evolution of the island width is plotted for different  $\chi_{\parallel}$  and  $\chi_{\perp}$ . The results are intuitive, i.e. a smaller  $\chi_{\parallel}$  or larger  $\chi_{\perp}$  can eliminate the oscillation. This is because a smaller  $\chi_{\parallel}/\chi_{\perp}$  can lower the energy transport level along the magnetic field lines, which would reduce the variation of  $\delta\nabla_{\parallel}p$  term when the size of magnetic island changes.

#### 4. Summary and discussion

The initial value code MDC (MHD@Dalian Code) is upgraded with the capability of two-fluid effects. On the basis of the well-known four-field equations [40], the bootstrap current, parallel and perpendicular transport effects are additionally included. In this paper, the numerical simulation on the mode penetration is conducted based on the two-fluid model. Main points can be summarized as follows.

- (i) The threshold of mode penetration at zero rotation is explored. It is found that for the classical TM ( $f_b = 0$ ), there is not a threshold for mode penetration. At this circumstance, the behavior of magnetic island is dominated by driven reconnection, i.e. the saturated island width is positively related to the amplitude of RMP. For the NTM ( $f_b = 0$ ), on the other hand, a mode penetration like phenomenon is observed consisting of a driven reconnection regime and a NTM regime. This phenomenon is different from the so-called mode penetration, but can be mistakenly defined as mode penetration if not carefully distinguished. It may provide a possible explanation for the finite mode penetration threshold at zero rotation detected in experiments.
- (ii) The effect of diamagnetic drift flow on the mode penetration is numerically studied. For a smaller diamagnetic drift flow, numerical results show that its influence is almost the same as the electric drift flow with comparable frequency. However, for a larger diamagnetic drift flow, it can drive a stabilizing effect on the magnetic island through the  $\delta\nabla_{\parallel}p$  term in equation (2). Besides, an oscillation phenomenon of the island width is observed. This oscillation is linked with the change of pressure

during the variation of island width. It tends to appear in the high Lundquist number  $S$  and high  $\chi_{\parallel}/\chi_{\perp}$  regime, where the parameter of advanced tokamak exactly lies in.

It should be pointed out that, in our simulation, the resistivity  $\eta$  is set as a constant. On more realistic regards,  $\eta$  is related to the temperature and can be estimated by the following equation

$$\eta \approx \frac{\pi e^2 m^{1/2}}{(4\pi\epsilon_0)^2 (KT_e)^{3/2}} \ln \Lambda, \quad (8)$$

where  $\ln \Lambda$  is a correction factor due to small-angle collisions and is approximate to 16 in fusion plasmas. In addition, bremsstrahlung radiation of ions and impurities inside the magnetic island [46] can radiate considerable energy and make significant modification to the pressure profile, which can directly affect the bootstrap current and increase the resistivity inside the island. These effects will be included in our future study.

## Acknowledgements

We acknowledge the Super Computer Center of Dalian University of Technology for providing computer resources. This work is supported by National Natural Science Foundation of China (Grant Nos. 11925501 and 12075048) and Fundamental Research Funds for the Central Universities (Grant No. DUT21GJ204).

## References

- [1] Furth H P, Killeen J and Rosenbluth M N 1963 *The Physics of Fluids* **6** 459–484 (Preprint <https://aip.scitation.org/doi/pdf/10.1063/1.1706761>) URL <https://aip.scitation.org/doi/abs/10.1063/1.1706761>
- [2] Rutherford P H 1973 *The Physics of Fluids* **16** 1903–1908 (Preprint <https://aip.scitation.org/doi/pdf/10.1063/1.1694232>) URL <https://aip.scitation.org/doi/abs/10.1063/1.1694232>
- [3] Carrera R, Hazeltine R D and Kotschenreuther M 1986 *The Physics of Fluids* **29** 899–902 (Preprint <https://aip.scitation.org/doi/pdf/10.1063/1.865682>) URL <https://aip.scitation.org/doi/abs/10.1063/1.865682>
- [4] Bardóczi L, Rhodes T L, Bañón Navarro A, Sung C, Carter T A, La Haye R J, McKee G R, Petty C C, Chrystal C and Jenko F 2017 *Physics of Plasmas* **24** 056106 (Preprint <https://doi.org/10.1063/1.4977533>) URL <https://doi.org/10.1063/1.4977533>
- [5] Wang Z X, Wei L and Yu F 2015 *Nuclear Fusion* **55** 043005 URL <https://doi.org/10.1088/0029-5515/55/4/043005>
- [6] Zhang W, Ma Z W, Zhu J and Zhang H W 2019 *Plasma Physics and Controlled Fusion* **61** 075002 URL <https://doi.org/10.1088/1361-6587/ab16ae>
- [7] La Haye R J 2006 *Physics of Plasmas* **13** 055501 (Preprint <https://doi.org/10.1063/1.2180747>) URL <https://doi.org/10.1063/1.2180747>
- [8] Sauter O, Henderson M A, Ramponi G, Zohm H and Zucca C 2010 *Plasma Physics and Controlled Fusion* **52** 025002 URL <https://doi.org/10.1088/0029-5515/52/2/025002>
- [9] Maraschek M 2012 *Nuclear Fusion* **52** 074007 URL <https://doi.org/10.1088/0029-5515/52/7/074007>



- [10] Hender T, Fitzpatrick R, Morris A, Carolan P, Durst R, Edlington T, Ferreira J, Fielding S, Haynes P, Hugill J, Jenkins I, Haye R L, Parham B, Robinson D, Todd T, Valovic M and Vayakis G 1992 *Nuclear Fusion* **32** 2091–2117 URL <https://doi.org/10.1088%2F0029-5515%2F32%2F12%2Fi02>
- [11] Yu Q, Günter S and Finken K H 2009 *Physics of Plasmas* **16** 042301 (*Preprint* <https://doi.org/10.1063/1.3100236>) URL <https://doi.org/10.1063/1.3100236>
- [12] Buttery R, Benedetti M D, Gates D, Gribov Y, Hender T, Haye R L, Leahy P, Leuer J, Morris A, Santagiustina A, Scoville J, Tubbing B, Team J, Team C D R and Team D D 1999 *Nuclear Fusion* **39** 1827–1835 URL <https://doi.org/10.1088/0029-5515/39/11y/323>
- [13] Lanctot M, Olofsson K, Capella M, Humphreys D, Eidietis N, Hanson J, Paz-Soldan C, Strait E and Walker M 2016 *Nuclear Fusion* **56** 076003 URL <https://doi.org/10.1088/0029-5515/56/7/076003>
- [14] Logan N, Zhu C, Park J K, Yang S and Hu Q 2021 *Nuclear Fusion* **61** 076010 URL <https://doi.org/10.1088/1741-4326/abff05>
- [15] Nave M and Wesson J 1990 *Nuclear Fusion* **30** 2575–2583 URL <https://doi.org/10.1088/0029-5515/30/12/011>
- [16] Lu S S, Ma Z W, Zhang H W and Liu Y 2020 *Plasma Physics and Controlled Fusion* **62** 125005 URL <https://doi.org/10.1088/1361-6587/abbc4>
- [17] Wang H, Wang Z, Ding Y and Rao B 2015 *Plasma Science and Technology* **17** 539–544 URL <https://doi.org/10.1088/1009-0630/17/7/03>
- [18] Wolf R, Biel W, Bock M D, Finken K, Günter S, Hogeweij G, Jachmich S, Jakubowski M, Jaspers R, Krmer-Flecken A, Koslowski H, Lehnen M, Liang Y, Unterberg B, Varshney S, von Hellermann M, Yu Q, Zimmermann O, Abdullaev S, Donné A, Sann U, Schweer B, Tokar M, Westerhof E and the TEXTOR Team 2005 *Nuclear Fusion* **45** 1700–1707 URL <https://doi.org/10.1088/0029-5515/45/12/026>
- [19] Choi W, La Haye R J, Lanctot M J, Olofsson K E, Strait E J, Sweeney R and Volpe F A 2018 *Nuclear Fusion* **58** aaa6e3 ISSN 17414326 URL <https://doi.org/10.1088/1741-4326/aaa6e3>
- [20] Tang W, Wang Z X, Wei L, Wang J and Lu S 2020 *Nuclear Fusion* **60** 026015 URL <https://doi.org/10.1088/1741-4326/ab61d5>
- [21] Nelson A O, Logan N C, Choi W, Strait E J and Kolemen E 2020 *Plasma Physics and Controlled Fusion* **62** 094002 URL <https://doi.org/10.1088/1361-6587/ab9b3b>
- [22] Fitzpatrick R 1993 *Nuclear Fusion* **33** 1049–1084 URL <https://doi.org/10.1088/0029-5515/33/7/i08>
- [23] Yu Q and Günter S 2008 *Nuclear Fusion* **48** 065004 URL <https://doi.org/10.1088/0029-5515/48/6/065004>
- [24] Cole A J, Hegna C C and Callen J D 2007 *Phys. Rev. Lett.* **99**(6) 065001 URL <https://link.aps.org/doi/10.1103/PhysRevLett.99.065001>
- [25] Wang J, Wang Z X and Wei L 2015 *Physics of Plasmas* **22** 092122 (*Preprint* <https://doi.org/10.1063/1.4931067>) URL <https://doi.org/10.1063/1.4931067>
- [26] Beidler M T, Callen J D, Hegna C C and Sovinec C R 2018 *Physics of Plasmas* **25** 082507 (*Preprint* <https://doi.org/10.1063/1.5046076>) URL <https://doi.org/10.1063/1.5046076>
- [27] Zhang H W, Lin X, Ma Z W, Zhang W and Bagwell T E 2021 *Plasma Physics and Controlled Fusion* **63** 035011 URL <https://doi.org/10.1088/1361-6587/abd304>
- [28] Becoulet M, Orain F, Maget P, Mellet N, Garbet X, Nardon E, Huysmans G, Casper T, Loarte A, Cahyna P, Smolyakov A, Waelbroeck F, Schaffer M, Evans T E, Liang Y, Schmitz O, Beurskens M, Rozhansky V and Kaveeva E 2012 *Nuclear Fusion* **52** 054003 URL <http://doi.org/10.1088/0029-5515/52/5/054003>
- [29] Yu Q, Günter S and Lackner K 2018 *Nuclear Fusion* **58** 054003 URL <https://doi.org/10.1088/1741-4326/2Faab2fb>
- [30] Fitzpatrick R 2018 *Physics of Plasmas* **25** 082513 (*Preprint* <https://doi.org/10.1063/1.5043203>) URL <https://doi.org/10.1063/1.5043203>

- [31] Fitzpatrick R 2018 *Physics of Plasmas* **25** 112505 (Preprint <https://doi.org/10.1063/1.5053804>) URL <https://doi.org/10.1063/1.5053804>
- [32] Yu Q, Günter S and Lackner K 2021 *Nuclear Fusion* **61** 036040 URL <https://doi.org/10.1088/1741-4326/abd197>
- [33] Hu Q, Logan N, Park J K, Paz-Soldan C, Nazikian R and Yu Q 2020 *Nuclear Fusion* **60** 076006 URL <https://doi.org/10.1088/1741-4326/ab8b79>
- [34] Bock M D, Classen I, Busch C, Jaspers R, Koslowski H and and B U 2008 *Nuclear Fusion* **48** 015007 URL <https://doi.org/10.1088/0029-5515/48/1/015007>
- [35] Wei L, Wang Z X, Wang J and Yang X 2016 *Nuclear Fusion* **56** 106015 URL <http://stacks.iop.org/0029-5515/56/i=10/a=106015?key=crossref.51a4d6ebf40ee4461b4ad0b15ca7f588>
- [36] Wang J, Wang Z X, Wei L and Liu Y 2017 *Nuclear Fusion* **57** 046007 URL <http://stacks.iop.org/0029-5515/57/i=4/a=046007?key=crossref.6d879fa2ab17585f1e3b54ac2dcce45b>
- [37] Liu T, Wang Z X, Wang J and Wei L 2018 *Nuclear Fusion* **58** 076026 URL <https://doi.org/10.1088%2F1741-4326%2Faac527>
- [38] Ye C, Wang Z X, Wei L and Hu Z Q 2019 *Nuclear Fusion* **59** 096044 URL <http://iopscience.iop.org/10.1088/1741-4326/ab3000>
- [39] Han M, Wang Z X, Dong J and Du H 2017 *Nuclear Fusion* **57** 046019 URL <https://doi.org/10.1088/1741-4326/aa5d02>
- [40] Hazeltine R D, Kotschenreuther M and Morrison P J 1985 *The Physics of Fluids* **28** 2466–2477 (Preprint <https://aip.scitation.org/doi/pdf/10.1063/1.865255>) URL <https://aip.scitation.org/doi/abs/10.1063/1.865255>
- [41] Bickerton R J, Connor J W and Taylor J B 1971 *Nature Physical Science* **229** 110–112 URL <https://doi.org/10.1038/physci229110a0>
- [42] Kikuchi Y, De Bock M F M, Finken K H, Jakubowski M, Jaspers R, Koslowski H R, Kraemer-Flecken A, Lehnen M, Liang Y, Matsunaga G, Reiser D, Wolf R C and Zimmermann O (TEXTOR-team) 2006 *Phys. Rev. Lett.* **97**(8) 085003 URL <https://link.aps.org/doi/10.1103/PhysRevLett.97.085003>
- [43] Hu Q, Yu Q, Rao B, Ding Y, Hu X and Zhuang G 2012 *Nuclear Fusion* **52** 083011 URL <http://doi.org/10.1088/0029-5515/52/8/083011>
- [44] Tang W, Wei L, Wang Z, Wang J, Liu T and Zheng S 2019 *Plasma Science and Technology* **21** 065103 URL <https://doi.org/10.1088%2F2058-6272%2Fab0a18>
- [45] Fitzpatrick R 1998 *Physics of Plasmas* **5** 3325–3341 (Preprint <https://doi.org/10.1063/1.873000>) URL <https://doi.org/10.1063/1.873000>
- [46] Gates D A and Delgado-Aparicio L 2012 *Phys. Rev. Lett.* **108**(16) 165004 URL <https://link.aps.org/doi/10.1103/PhysRevLett.108.165004>